Utilization of Photon Orbital Angular Momentum in the Low-Frequency Radio Domain

B. Thidé,[1,*] H. Then,[2] J. Sjöholm,[3] K. Palmer,[3] J. Bergman,[1] T. D. Carozzi,[4] Ya. N. Istomin,[5] N. H. Ibragimov,[6] and R. Khamitova[6]

[1]*Swedish Institute of Space Physics, Ångström Laboratory, P.O. Box 537, SE-751 21 Uppsala, Sweden*
[2]*Institute of Physics, Carl-von-Ossietzky Universität Oldenburg, D-261 11 Oldenburg, Germany*
[3]*Department of Astronomy and Space Physics, Ångström Laboratory, P.O. Box 515, SE-751 20 Uppsala, Sweden*
[4]*Astronomy and Astrophysics Group, Department of Physics and Astronomy, University of Glasgow, Glasgow, G12 8QQ, Scotland, United Kingdom*
[5]*I. E. Tamm Theory Department, P. N. Lebedev Physical Institute, 53 Leninsky Prospect, Moscow, 119991, Russia*
[6]*Department of Mathematics and Science, Research Centre ALGA: Advances in Lie Group Analysis, Blekinge Institute of Technology, SE-371 79 Karlskrona, Sweden*

(Received 21 May 2007; published 22 August 2007)

We show numerically that vector antenna arrays can generate radio beams that exhibit spin and orbital angular momentum characteristics similar to those of helical Laguerre-Gauss laser beams in paraxial optics. For low frequencies ($\lesssim 1$ GHz), digital techniques can be used to coherently measure the instantaneous, local field vectors and to manipulate them in software. This enables new types of experiments that go beyond what is possible in optics. It allows information-rich radio astronomy and paves the way for novel wireless communication concepts.

DOI: 10.1103/PhysRevLett.99.087701 PACS numbers: 84.40.Ba, 07.57.−c, 42.25.Ja, 95.85.Bh

Classical electrodynamics exhibits a rich set of symmetries [1], and to each Lie symmetry there corresponds a conserved quantity [2,3]. Commonly utilized conserved electromagnetic (EM) quantities are the energy and linear momentum, where the underlying symmetries, under Poincaré transformations, are homogeneity in time and in space, respectively.

Another conserved quantity, manifesting the isotropy of space, is the EM angular momentum, whose mechanical properties were predicted theoretically in 1909 [4] and demonstrated experimentally in 1936 [5]. A collection of nonrelativistic, spinless, classical particles with linear momenta $\mathbf{p}_i^{\mathrm{mech}}$ has angular momentum $\mathbf{J}^{\mathrm{mech}} = \sum_i (\mathbf{x}_i - \mathbf{x}_0) \times \mathbf{p}_i^{\mathrm{mech}}$, where $\mathbf{x}_0$ is the moment point. When this system interacts with EM radiation with spin angular momentum (SAM) $\mathbf{S}^{\mathrm{EM}}$ and EM orbital angular momentum (OAM) $\mathbf{L}^{\mathrm{EM}}$, the total angular momentum, $\mathbf{J}^{\mathrm{tot}} = \mathbf{J}^{\mathrm{mech}} + \mathbf{J}^{\mathrm{EM}}$, where $\mathbf{J}^{\mathrm{EM}} = \mathbf{S}^{\mathrm{EM}} + \mathbf{L}^{\mathrm{EM}} = \varepsilon_0 \int d^3x (\mathbf{x} - \mathbf{x}_0) \times (\mathbf{E} \times \mathbf{B})$, is conserved [6]. Hence, for a fixed $\mathbf{S}^{\mathrm{EM}}$, a change in $\mathbf{J}^{\mathrm{mech}}$ will result in an opposite change in $\mathbf{L}^{\mathrm{EM}}$, observed as a rotational (azimuthal) Doppler shift [7]. This shift is distinct from the translational Doppler shift, which is a manifestation of the conservation of linear momentum. As shown in Ref. [8], using an angular momentum flux representation [9], in a beam geometry it is possible to separate $\mathbf{J}^{\mathrm{EM}}$ into $\mathbf{S}^{\mathrm{EM}}$, which depends only on the local polarization structure, and $\mathbf{L}^{\mathrm{EM}}$, which depends on the gradient of the fields; see also Ref. [10].

During the past few decades the use of EM OAM (beam vorticity) has come to the fore in optics [11] and in atomic and molecular physics [12]. However, while SAM (wave polarization), generated by proper phasing of the two legs in a crossed dipole or by using helix antennas, has been used routinely for at least half a century, OAM has not yet been utilized to any significant degree in radio physics [13] or its applications such as radio astronomy [14]. The use of radio OAM is currently being contemplated for detection of ultrahigh energy neutrinos interacting with the moon [15], studies of radio wave interactions with the atmosphere and ionosphere [16–18], and radar probing of the sun [19,20].

We propose to use antenna arrays for generating and detecting both SAM and OAM in radio beams and show numerically how this works. In such arrays one needs access to the complete 3D vectors of the radio EM field over an area which is large enough to intersect a substantial fraction of the radio beam. This requires vector antennas, e.g., tripoles [21,22]; crossed dipole antennas will be useful for beam directions nearly perpendicular to the antenna planes. Using digital samplers connected directly to each vector antenna, the local, instantaneous 3D radio field vectors themselves can be measured coherently up to the gigahertz range, enabling their manipulation, including $\mathbf{J}^{\mathrm{EM}}$ processing, entirely in software. This is in contrast to infrared and optical frequencies for which current detectors are incapable of measuring first-order field quantities. There phase-coherent down-conversion to the low-frequency radio domain might provide a solution.

Lasers often use Laguerre-Gaussian (LG) modes [23] in which the phases of the electric and magnetic vector fields in a plane perpendicular to the beam axis have an $l\varphi$ dependence where l is an integer and φ is the azimuthal angle. This means that for $l \neq 0$ the phase fronts of LG modes are not planar but helical. As shown in Ref. [24], this implies that LG beams carry an OAM of $l\hbar$ per photon. In the paraxial approximation, the LG modes form a complete basis set for light beams [23].

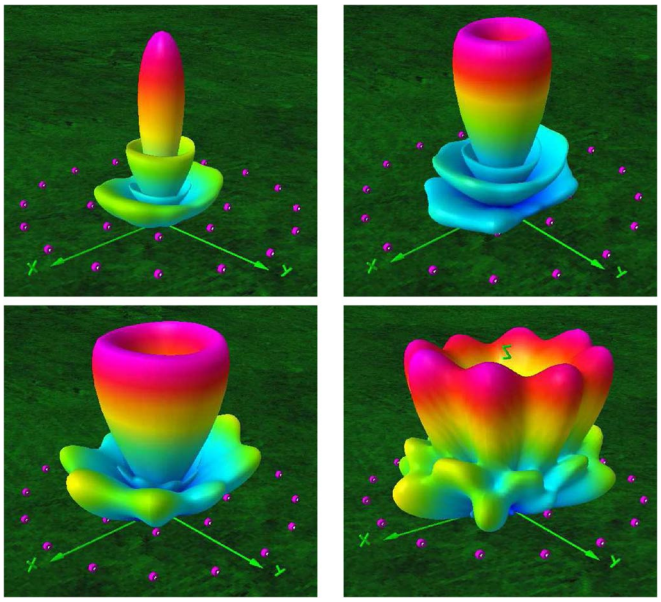

FIG. 1 (color online). Radiation patterns for radio beams generated by one circle of 8 antennas and radius λ plus a concentric circle with 16 antennas and radius 2λ; all antennas are 0.25λ over the ground. Notice the influence of l on the radiation pattern. Here $l = 0$ (upper left), $l = 1$ (upper right), $l = 2$ (lower left), and $l = 4$ (lower right).

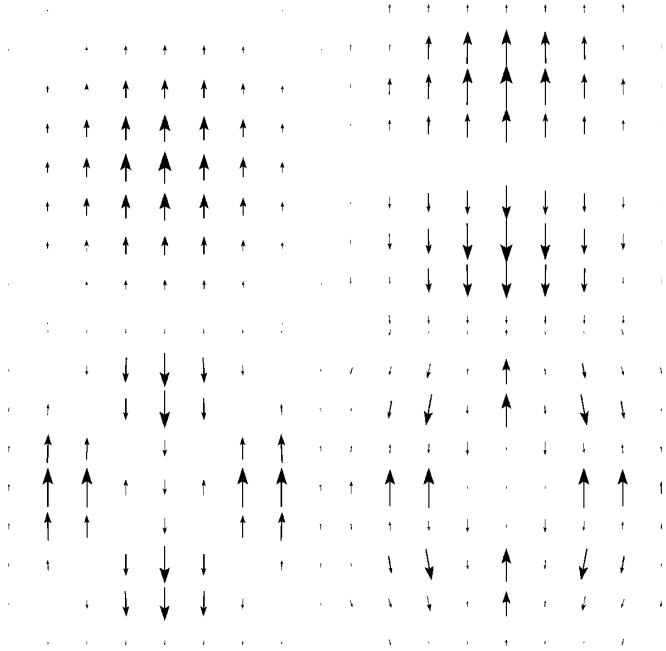

FIG. 2. Samples of instantaneous electric field vectors **E** across the main lobes of the beams in Fig. 1 (same l values and plotting order). The size of an arrow is linearly proportional to the local $|\mathbf{E}|$. As expected for OAM carrying beams, the phase of the EM field changes by $l2\pi$ for a full turn around the beam axis.

A pure OAM state radio beam of frequency ω and energy H has a beam axis OAM component $L_z^{\mathrm{EM}} = lH/\omega$ and the fields have an azimuthal phase dependence of $\exp(il\varphi)$, where l is an integer as in a LG beam. In order to study the possibility of using OAM in radio, we consider an antenna array and assume for simplicity that each antenna is located equidistantly along the perimeters of circles (see Fig. 1). The antennas are fed the same signal, but successively delayed relative to each other such that after a full turn around the antenna array axis, the phase has been incremented by $l2\pi$. The far field intensity patterns, calculated with the software package NEC2 [25] which solves Maxwell's equations for a given set of antenna currents, are displayed in Figs. 1, 3, and 4, and are very similar to those obtained in paraxial optics. Figure 2 displays the instantaneous **E** field vectors across the main lobes for different l. Theory predicts that $j = l + s = \omega J_z^{\mathrm{EM}}/H$ [24]. Table I lists the results obtained for $l = 0, 1, 2, 3$ and $s = -1$ for a radio beam generated by an antenna array. The agreement is excellent.

The superposition of two coaxial OAM states was modeled numerically by using two concentric antenna rings with different radii. In the inner ring we increase the overall phase between successive antennas by $2\pi l_1/n_1$. In the outer ring we use the phase increment $2\pi l_2/n_2$. The variables n_1 and n_2 are the number of antennas in each ring, respectively, and l_1 and l_2 are the phase increment factors corresponding to the OAM number l in the LG beams. The resulting antenna radiation patterns are shown in Fig. 3 for three different combinations of l_1 and l_2. These patterns would be difficult to synthesize without resorting to the OAM technique. For comparison, intensity patterns for OAM carrying LG beams for the same l_1 and l_2 combinations are also shown.

In the general (linear) case, the total OAM in a beam is a superposition of several OAM states. This superposition can be decomposed into pure OAM states via a discrete Fourier transform. In particular, one has to integrate the complex field vector weighted with $\exp(-il\varphi)$ along a circle around the beam axis. Since there will be only a finite number of antennas along the integration path, there is an upper limit on the largest OAM number that can be resolved. Namely, $|l| < N/2$, where N is the number of antennas on a circle around the beam axis. We have assumed that the beam axis is centered on the antenna array, but this is not necessarily true. The beam axis is determined by the emitter only, not by the receiving antenna array. Therefore an incoming radio beam might not

TABLE I. Scaling of $\omega J_z^{\mathrm{EM}}/H$ as a function of l for a right-hand circular polarized beam ($s = -1$) formed by a ring array of 10 crossed dipoles. Array radius $D = \lambda$, antennas 0.1λ over perfect ground, polar angle $\theta = 0$.

l	s	$j = l + s$	$\omega J_z^{\mathrm{EM}}/H$
0	−1	−1	−1.019
1	−1	0	−0.022
2	−1	1	0.971
3	−1	2	1.81

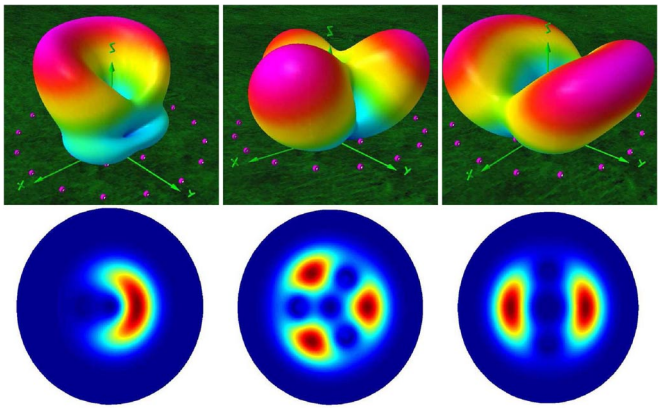

FIG. 3 (color online). Beams obtained by superimposing two different OAM states. The upper three panels show the radiation patterns for the antenna array, and the lower three panels show the corresponding intensity patterns, head on, calculated for Laguerre-Gaussian beams. The leftmost are for $l_1 = 1$ and $l_2 = 2$, the middle ones are for $l_1 = 1$ and $l_2 = 4$, and the rightmost are for $l_1 = 2$ and $l_2 = 4$. Notice the good agreement between the patterns obtained with the antenna array model and the paraxial LG beam model.

overlap the antenna array perfectly so that only an asymmetric spatial part of the beam can be analyzed. A disadvantage in this case is that we do not have exact information of the phase along the whole circle around the beam axis. We have to extrapolate from accurate measurements of the field vectors within the finite size antenna array to the field vectors around the beam axis. This extrapolation yields an uncertainty $\Delta l > R\Delta\varphi/D$ ($R \gg D$), where $\Delta\varphi$ is the smallest phase difference in radians that can be resolved, D is the diameter of the antenna array, and R is the distance from the beam axis to the antenna array. Since l is integer valued, the uncertainty does not matter as long as it is less than $1/2$. While losing information about the individual OAM states, it is possible to measure estimated larger OAM numbers up to $|l| < K\pi R/D$ ($R \gg D$), where K is the number of antennas along a circle segment of length D.

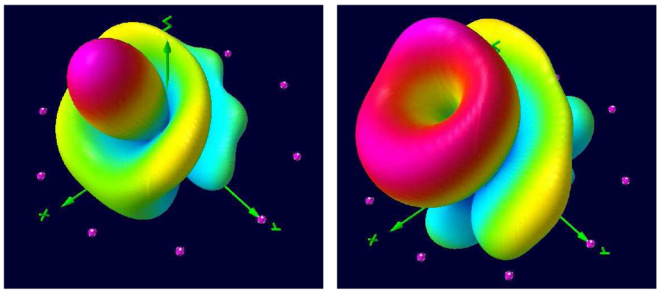

FIG. 4 (color online). Radiation patterns for a circularly polarized beam propagating obliquely ($\theta = 25°$) with $l = 0$ (left) and $l = 1$ (right), generated by phasing the individual elements of a ten-tripole array in free space. This illustrates that with a tripole array it is possible to control electronically both the beam direction and l. This is not possible with arrays of single or crossed dipoles. Note that for $l \neq 0$, there will be an on-beam-axis minimum which can be useful to block out a bright object when observing faint surrounding objects [31], e.g., in the solar corona [20].

The Poynting vector of a radio beam with OAM has a helical phase structure and spirals around the main beam axis with a pitch angle $\alpha_l = \arctan(\lambda l/2\pi R)$. This angle can be resolved if l can be resolved, i.e., if $\Delta l < 1/2$. In this case one observes multiple images of a single point source where each image corresponds to a pure OAM state l. If l cannot be resolved, the multiple images blend together yielding a smeared spot. Conversely, if the individual OAM states are resolved, the smeared spots are resolved as multiple images (one for each l), enabling self-calibration techniques that sharpen the radio image via the use of OAM.

Inserting typical values of $D = 100$ km, $\Delta\varphi = 2\pi \times 1°/360°$, into $\Delta l > R\Delta\varphi/D$, and requiring that $\Delta l < 1/2$, one obtains $R_{\max} = 3000$ km for which the OAM can be resolved. It should therefore be possible to probe OAM processes in the Earth's ionosphere and lower magnetosphere and also to actively induce plasma vorticity and strong toroidal electric currents there [16]. In particular, a radio beam that interacts with a turbulent medium will carry information on the vorticity of this medium allowing for remote radio imaging of the turbulence [17]. But, it is not likely that radio beams from distant astronomical objects are so narrowly focused that they can be probed for OAM unless the array extends into space. On the other hand, if the ionosphere adds OAM to a beam from a distant source, this added OAM can be measured and compensated for.

Should, however, the radio emitting object rotate fast and have sharp discrete lines in its emission spectrum, the angular momentum of the emitted EM waves can be measured indirectly via shifts and splittings of the spectral lines. The shifts result from the rotational Doppler effect $\omega - \omega_0 = (l + s)\Omega_\parallel$ where $\Omega_\parallel$ is the projection of the rotation frequency onto the wave vector $\mathbf{k}$ [7]. Decomposing into pure spin states, the discrete emission spectrum will be decomposed into one for $s = +1$ and one for $s = -1$. These two spectra should almost coincide in their spectral lines, except for an overall shift. The relative overall shift between the two spectra is equal to twice the rotational frequency of the emitter. Once $\Omega_\parallel$ has been read off, one can search for spectral lines that are separated exactly by $\Omega_\parallel$ (and integer multiples thereof). Each of these spectral lines corresponds to a specific OAM state.

When pointing the beam in a direction other than the z axis (orthogonal to the plane of the dipoles), vector sensing antennas such as tripoles are much preferred. They have the advantage that the three orthogonal antenna currents can be viewed as the x, y, and z components of a composite antenna current vector $\mathbf{j}(t, \mathbf{x})$ which, under software control, can be rotated into any given direction in space, in the receive case even after the fact. To generate off-zenith EM beams with nonzero l values, the tripole is indispensable

since one cannot control the direction of the beam with linear dipoles or crossed dipoles and still maintain the desired $l\varphi$ phase dependence; see Fig. 4. This is because the phase difference between the elements is used to point the beam. The only way to overcome this limitation would be to mechanically rotate the antenna array. Such an arrangement would be infeasible.

In summary, we have shown by theoretical and numerical modeling that a number of the photon SAM and OAM signatures observed in paraxial optics can be generated in the radio frequency range where, for low enough frequencies ($\lesssim 1$ GHz), modern digital radio techniques can be used to measure coherently the 3D electric (and magnetic) vectors in the beams. This opens up new kinds of fundamental electromagnetic radiation experiments. Furthermore, minor changes of the design of the large low-frequency multiarray radio telescopes coming on line (LOFAR [26]) or in the planning stage (SKA [27]), would enable them to utilize not only SAM but also OAM, which would increase their resolution, sensitivity, interference tolerance, and overall usefulness. The LOIS (LOFAR outrigger in Scandinavia) test station in southern Sweden has already implemented the radio OAM techniques and is currently being set up for the first proof-of-concept experiments [19].

Since information can be encoded as OAM states [28] that span a much larger state space than the two-state SAM space [29], radio OAM techniques hold promise for the development of novel information-rich radar and wireless communication concepts and methodologies. Furthermore, it is conceivable that signatures related to radio OAM or other conserved quantities in Dirac's symmetrized form of the Maxwell-Lorentz EM theory might provide clues on the existence of magnetic monopoles [30]. Finally, it should be mentioned that invariants are very useful for assessing the stability and robustness of numerical simulation codes.

The authors thank Sir Michael Berry, Bruce Elmegreen, Bengt Eliasson, Erik B. Karlsson, Dan Stinebring, and Willem Baan for elucidating discussions and helpful comments. We gratefully acknowledge the financial support from the Swedish Governmental Agency for Innovation Systems (VINNOVA).

*Also at: LOIS Space Centre, Växjö University, SE-351 95 Växjö, Sweden.
bt@irfu.se

[1] M. Ribarič and L. Šušteršič, *Conservation Laws and Open Questions of Classical Electrodynamics* (World Scientific, Singapore, 1990).
[2] E. Noether, Nachr. Ges. Wiss. Goettingen, Math. Phys. Kl. **1**, 235 (1918) [Transp. Theory Stat. Phys. **1**, 186 (1971)].
[3] N. H. Ibragimov, J. Math. Anal. Appl. **333**, 311 (2007).
[4] J. H. Poynting, Proc. R. Soc. A **82**, 560 (1909).
[5] R. A. Beth, Phys. Rev. **50**, 115 (1936).
[6] C. Cohen-Tannoudji, J. Dupont-Roc, and G. Grynberg, *Photons and Atoms: Introduction to Quantum Electrodynamics* (John Wiley & Sons, New York, 1989), Chap. 1.
[7] J. Courtial, D. A. Robertson, K. Dholakia, L. Allen, and M. J. Padgett, Phys. Rev. Lett. **81**, 4828 (1998).
[8] S. M. Barnett, J. Opt. B **4**, S7 (2002).
[9] J. Schwinger, L. L. DeRaad, Jr., K. A. Milton, and W. Tsai, *Classical Electrodynamics* (Perseus, Reading, MA, 1998), Chap. 2.
[10] M. V. Berry, in *Singular Optics*, edited by M. S. Soskin, SPIE Proceedings Vol. 3487 (SPIE-International Society for Optical Engineering, Bellingham, WA, 1998), pp. 6–11.
[11] L. Allen, J. Opt. B **4**, S1 (2002).
[12] C. N. Cohen-Tannoudji, Rev. Mod. Phys. **70**, 707 (1998).
[13] S. H. Krishnamurthy, A. Konanur, G. Lazzi, and B. L. Hughes, in *Proceedings of the 38th Asilomar Conference on Signals, Systems and Computers, 2004* (IEEE, New York, 2004), Vol. 1, pp. 1237–1241.
[14] M. Harwit, Astrophys. J. **597**, 1266 (2003).
[15] O. Stål, J. Bergman, B. Thidé, L. K. S. Daldorff, and G. Ingelman, Phys. Rev. Lett. **98**, 071103 (2007).
[16] Y. N. Istomin, Phys. Lett. A **299**, 248 (2002).
[17] C. Paterson, Phys. Rev. Lett. **94**, 153901 (2005).
[18] B. Thidé, E. N. Sergeev, S. M. Grach, T. B. Leyser, and T. D. Carozzi, Phys. Rev. Lett. **95**, 255002 (2005).
[19] B. Thidé, in *Mathematical Modelling of Wave Phenomena*, edited by B. Nilsson and L. Fisherman (Växjö University Press, Växjö, Sweden, 2004), pp. 315–331.
[20] M. V. Khotyaintsev, V. N. Mel'nik, B. Thidé, and O. O. Konovalenko, Sol. Phys. **234**, 169 (2006).
[21] R. Compton, Jr., IEEE Trans. Antennas Propag. **29**, 944 (1981).
[22] T. Carozzi, R. Karlsson, and J. Bergman, Phys. Rev. E **61**, 2024 (2000).
[23] A. E. Siegman, *Lasers* (University Science Books, Sausalito, CA, 1986), Chap. 16.
[24] L. Allen, M. W. Beijersbergen, R. J. C. Spreeuw, and J. P. Woerdman, Phys. Rev. A **45**, 8185 (1992).
[25] NEC2, Numerical Electromagnetic Code, Version 2, http://www.nec2.org.
[26] Low Frequency Array (LOFAR), http://www.lofar.org.
[27] Square Kilometre Array (SKA), http://www.skatelescope.org.
[28] G. Gibson, J. Courtial, M. J. Padgett, M. Vasnetsov, V. Pas'ko, S. M. Barnett, and S. Franke-Arnold, Opt. Express **12**, 5448 (2004).
[29] J. Leach, M. J. Padgett, S. M. Barnett, S. Franke-Arnold, and J. Courtial, Phys. Rev. Lett. **88**, 257901 (2002).
[30] N. H. Ibragimov, R. Khamitova, and B. Thidé, J. Math. Phys. (N.Y.) **48**, 053523 (2007).
[31] G. A. Swartzlander, Jr., Opt. Lett. **26**, 497 (2001).